Free-Carrier Generation in Aggregates of Single-Wall Carbon Nanotubes by Photoexcitation in the Ultraviolet Regime

Jared J. Crochet,[1,*] Sajjad Hoseinkhani,[2,†] Larry Lüer,[3] Tobias Hertel,[4] Stephen K. Doorn,[1] and Guglielmo Lanzani[5]

[1]*Center for Integrated Nanotechnologies, Los Alamos National Laboratory, Los Alamos, New Mexico 87545, USA*

[2]*CNR/INFM-ULTRAS, Politecnico di Milano, Milan 20133, Italy*

[3]*Madrid Institute of Advanced Studies, IMDEA Nanociencia, Madrid 28049, Spain*

[4]*Institute for Physical and Theoretical Chemistry Department of Chemistry and Pharmacy, University of Würzburg, Würzburg 97074, Germany*

[5]*Center for Nanoscience and Technology of IIT @ POLIMI and Physics Department of Politecnico di Milano, Milan 20133, Italy*

(Received 20 May 2011; published 16 December 2011)

We present evidence for the generation of free carriers in aggregated single-wall carbon nanotubes by photoexcitation in the energetic range of the $\pi \rightarrow \pi^*$ transition associated with the M saddle point of the graphene lattice. The underlying broad absorption culminating at 4.3 eV can be fit well with a Fano line shape that describes strong coupling of a saddle-point exciton to an underlying free electron-hole pair continuum. Moreover, it is demonstrated that transitions in this energetic region autoionize into the continuum by detecting features unique to the presence of free charges in the transient transmission spectra of the continuum-embedded second sub-band exciton, S_2.

DOI: 10.1103/PhysRevLett.107.257402 PACS numbers: 78.67.Ch, 61.48.De, 78.40.Ri, 78.67.Sc

Single-wall carbon nanotubes (SWNTs) can be thought of as circumferentially quantized graphene tubules whose electronic properties depend strongly on chirality[1]. The primary photoexcitations of unaggregated semiconducting tubes consist of several manifolds of highly anisotropic, strongly bound excitons [2]. It is known, however, that in semiconducting SWNTs the free-carrier response increases as a function of aggregate size [3]. From a phenomenological perspective, this observation can be interpreted as screening of the quasi-1D Coulomb interaction that leads to an enhanced response of the free-carrier continuum [4]. In SWNTs, this increase in the continuum optical response culminates at an ≈ 4.5 eV $\pi \rightarrow \pi^*$ transition arising from the graphene M saddle point [5]. Interestingly, the M-point transition in graphene is largely affected by excitonic effects [6] and gives rise to a Fano line shape absorbance that strongly alters the universal optical conductance of $\pi e^2/2h$ above the infrared spectral range [7,8]. It is understood that this exciton is extremely short-lived (< 1 fs), undergoing autoionization into the underlying free-carrier continuum. Nevertheless, the nature and role that the M-point transition as well as free carriers have in the photophysics of SWNTs in isolated and aggregated form is of fundamental and applied interest [9,10].

Here, we present a series of excitation-energy-dependent transient transmission ($\Delta T/T_0$) experiments on predominantly aggregated (6,5) SWNTs (CoMoCAT SG-65) embedded in a thin film gelatin matrix[11,12]. We find $\Delta T/T_0$ under UV excitation near the M point, where the electronic density of states is the largest [13] and differs strongly from resonant S_1 or S_2 excitation. A Fano line shape absorption of the M-point transition as well as a dynamic Stark shift coupled with a strong photoinduced absorption of the continuum-embedded S_2 exciton provide strong evidence for the photogeneration of free charges via autoionization upon UV excitation. This investigation experimentally illustrates how electronic dimensionality can be altered in a SWNT aggregate by nearest-neighbor interactions through charge transfer excitons [14] and emphasizes the prospect of SWNT networks for light harvesting applications.

A standard pump-probe configuration was used to measure differential transient transmission $\Delta T/T_0$. The experimental setup includes an amplified Ti:sapphire laser (200 μJ–1 kHz: 150 fs) that drives two nonlinear optical parametric amplifiers. A white light continuum was generated by focusing a fraction of the fundamental beam on a thin sapphire plate. The continuum was amplified in a barium borate crystal by pumping with the second harmonic at 390 nm. Broadband pulses were generated in visible, 1.8–2.4 eV, and infrared, 0.82–1.4 eV, spectral ranges and compressed on a set of doubly chirped mirrors to pulse widths of ≈ 10 and 15 fs, respectively. Excitation at 4.72 eV was provided by the third harmonic of the Ti:sapphire fundamental with a pulse width of ≈ 180 fs. The probe light consisted of the nonlinear optical parametric amplifier output or the white light continuum. Data acquisition was carried out via a computer-controlled optical multichannel analyzer that allowed for recording $\Delta T/T_0$ as a function of time delay between pump and probe pulses and as a function of probe wavelength.

Figure 1 shows the ground-state absorption spectrum of a SWNT gelatin film. The exciton resonances S_1–S_3 can be observed at 1.25, 2.16 [15], and 3.6 eV [16] residing on a broad background culminating at the $\pi \rightarrow \pi^*$ transition at

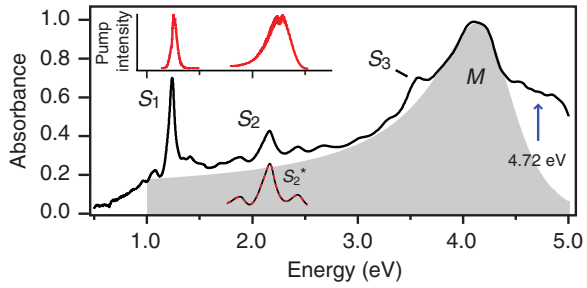

FIG. 1 (color). Absorption spectrum of SWNT sample. The exciton resonances S_i are labeled, and the grey shaded region is a Fano fit to the M-point exciton. The red dashed line indicated by S_2^* is a multipeak fit to the excitonic part of the S_2 region. The inset shows the excitation pulse spectra, and the blue arrow indicates third harmonic excitation.

approximately 4.3 eV. Motivated by recent investigations of the M-point exciton in graphene, we fit this feature with a Fano profile $A(E) \propto (q + \epsilon)^2/(1 + \epsilon^2)$, where $\epsilon = (E - E_r)/(\Gamma/2)$. Here, q^2 defines the ratio of the strength of the excitonic transition to the free $\pi \rightarrow \pi^*$ transition, E_r is the exciton resonance energy, and Γ corresponds to the exciton lifetime [7]. We find within this model that $E_r = 4.28$ eV, $\Gamma = 860$ meV (≈ 5 fs), and $q = -2.83$ fits the shape of the underlying absorbance sufficiently up to approximately 1 eV. This is similar to graphene, where at approximately 1 eV, the Fano tail no longer fits the optical conductivity [7]. Also, at higher energies than 4.5 eV, the absorbance is not very well-resolved because of strong absorption by the gelatin matrix. It is important to note that the E_r for this chirality range of SWNTs is approximately 700 meV smaller than what is measured in both single- and few-layer graphene, indicating, as predicted, that strong modifications in the $\pi \rightarrow \pi^*$ transition occur upon rolling the graphene sheet [5].

In Figs. 2(a)–2(c), time-resolved $\Delta T/T_0$ spectra in the vicinity of the S_2 exciton are shown in a color-coded representation. Here, strong photoinduced or excited-state absorption (PA, $\Delta T/T_0 < 0$) is shaded blue, and strong photobleach or ground-state bleaching (PB, $\Delta T/T_0 > 0$) is shaded red. Resonantly exciting the low-energy excitons ($S_1 - 1.4 \times 10^{15}$ photons/cm^2, $S_2 - 2.5 \times 10^{15}$ photons/cm^2 in Figs. 2(a) and 2(b), respectively), the apparent magnitude of the PA is smaller than the PB. In the specific case of resonantly exciting S_2, Fig. 2(b), we observed initially a broad PB which narrows down to the same width of Fig. 2(a) within approximately 50 fs. The initial broadening is caused by broadband excitation of energetically neighboring S_2 excitons [belonging to other impurity (n, m) species], in contrast to Fig. 2(a), where the excitation energy is resonant predominantly with the (6,5) tube. Hence, broadband excitation results in the resonant excitation of minority tube species through S_2, including the (6,4) and (8,3) tubes which initially contribute to the $\Delta T/T_0$ spectra. Recently, we have shown that the spectral

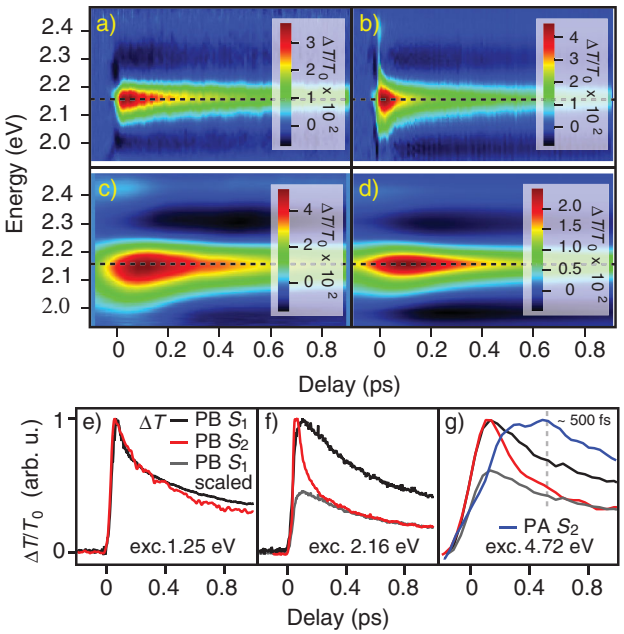

FIG. 2 (color). $\Delta T/T_0$ spectra around the S_2 (dashed line) after excitation at 1.25, 2.17, and 4.72 eV [(a)–(c), respectively]. The time resolution is approximately 10, 20, and 100 fs for (a)–(c). (d) shows a replica of (e) that has been convoluted by a 100 fs Gaussian along the time direction. Normalized $\Delta T/T_0$ traces in the maxima of the PB bands of S_1 and S_2 (red and black curves, respectively) exciting at 1.25, 2.15, and 4.72 eV are shown in (e)–(g). Grey traces in (f),(g) are replicas of the black traces scaled to match the red curves after initial relaxation, and the blue trace in (g) is the maximum of the PA band in (c).

narrowing observed here is caused by a two-step process that involves an S_2-to-S_1 internal conversion in ≈ 40 fs followed by resonance energy transfer from the minority tubes towards the majority (6,5) tube or towards other smaller band gap tubes within 10 fs [17]. We have also shown that the apparently delayed formation of the PA [Fig. 2(b)] occurs only in aggregates, while, in isolated tubes, the PA forms during the excitation pulse.

In contrast, exciting at 4.72 eV (8.3×10^{14} photons/cm^2), the PA and the PB have similar spectral weight at early delay times, and for longer times the PA becomes dominant in the $\Delta T/T_0$ spectra centered at ≈ 2.3 eV; see Fig. 2(c). Moreover, the maximum PA occurs after ≈ 500 fs, compared to ≈ 200 fs after resonantly exciting S_2 and less than 10 fs after resonantly exciting S_1. In order to further emphasize the difference between exciting at 4.72 eV and S_2, we show in Fig. 2(d) how the dynamics of resonant S_2 excitation appear after convolution with a 100 fs Gaussian pulse. As expected, the initial broadening is not resolved; however, clear differences between Fig. 2(c) and Fig. 2(d) remain. In Fig. 2(d), the maximum PA is reached within 200 fs and is stronger on the red side than on the blue side, as in Fig. 2(b). We can therefore conclude that UV excitation introduces an addi-

tional process which is superimposed on intertube energy-transfer effects observed at low-energy excitation.

Further insight is gained from analyzing the maximum PBs of S_1 and S_2 for different excitation conditions. As shown in Fig. 2(e), we find upon resonant excitation of S_1 that both PBs of S_1 and S_2 form together and decay similarly during the first 400 fs. However, resonantly exciting S_2 [Fig. 2(f)], we find a delayed rise of the PB of S_1 with a simultaneous decay of the PB of S_2, which was previously assigned to an ultrafast internal conversion of S_2 to S_1 [18]. Subsequently, the PBs S_1 and S_2 decay together, starting within approximately 200 fs, as shown by the scaled PB of S_1 (grey trace) in Fig. 2(f). For 4.72 eV excitation [Fig. 2(g)], similar to resonant S_2 excitation, we found a faster PB recovery of S_2 than of S_1. This is similar to what is observed while resonantly exciting S_2, but a closer look at the dynamics highlights an important difference. In Fig. 2(g), the time resolution is not as good as in Fig. 2(f) because of the longer excitation pulses at 4.72 eV, but it can be quite clearly observed that the time it takes for the two traces to reach a common decay is on the order of 500 fs, or approximately 2.5 times as much as in Fig. 2(f); see the grey trace in Fig. 2(g). This observation can be attributed to a delayed relaxation process that occurs predominantly in the S_2 spectral region only after exciting at higher energies and coincides with the maximum PA signal; see Fig. 2(g).

We performed a multi-Gaussian analysis of vertical cuts of Figs. 2(a)–2(c) at $t = 900$ fs (subsequent to energy transfer and internal conversion dynamics); see Figs. 3(a)–3(c). In the analysis, we simulated the PB by a scaled replica of the excitonic part of the ground-state absorption spectrum which represents ground-state bleaching while simulating the PA as an inversely scaled, broadened, and energetically shifted replica of the PB to represent excited-state absorption. Reasonable agreement was found for all the three excitation conditions. For low-energy excitation, redshifts of the PA less than 50 meV and small broadening values less than 100 meV were obtained, while, for UV excitation, a blueshift was observed of ≈ 60 meV and the broadening was very strong, in excess of 500 meV. The analysis suggests that there is a single PA band in the $\Delta T/T_0$ spectra, which is broader than PB and becomes dominant in the edges of the transient transmission spectrum, yielding $\Delta T/T_0 < 0$. As in quantum wells, this broadening of the excited state can be attributed to scattering of the exciton with the continuum in which it is embedded [19,20]. Supporting this conjecture, we found that the spectral position of the S_2 PB maximum for UV excitation, as opposed to low-energy excitation, was strongly time-dependent. As shown in Fig. 3(d), the PB was dynamically shifted with respect to the S_2 ground-state absorption energy and depended strongly on fluence. The S_2 PB was initially redshifted by 10 s of meV and within 20 ps was blueshifted to a maximum of 10 s of meV followed by a slow recovery back to the ground-state energy. In light of these three findings, which include a delayed relaxation pathway coinciding with an extremely broad strong PA and a fluence-dependent dynamic spectral shift of the S_2 PB, we discuss how photogenerated free carriers near the M point can alter the $\Delta T/T_0$ spectra near S_2 through charge transfer states.

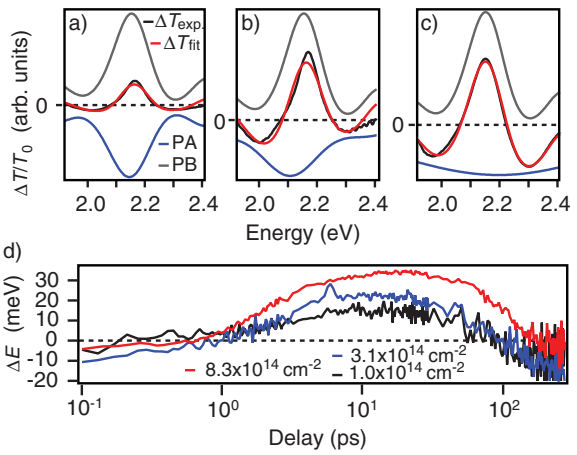

FIG. 3 (color). Decomposition of $\Delta T/T_0$ spectra at $t = 900$ fs for S_1, S_2, and 4.72 eV excitation [(a)–(c), respectively]. The PB contribution (grey curve) is a vertically scaled replica of the excitonic part of the ground-state absorption, while the PA contribution (blue curve) is calculated as an inverted, vertically scaled, shifted, and broadened replica of the PB contribution. (d) Fluence dependence of the dynamical shift of the S_2 PB exciting at 4.72 eV.

First, we ruled out the possibility of thermal or mechanical effects that could lead to our observations. If, upon the absorption of UV photons, the SWNT film underwent an increase in temperature, a spectral shift would be observed; however, as shown by Li *et al.* and Karaiskaj *et al.*, heating the (6,5) tube would result in a redshift of the transition energy which is mostly due to strain [21,22]. Moreover, in the absence of strain, it is predicted that the band gap of the (6,5) tube will be reduced upon a temperature increase [23]. Nonetheless, recent continuous-wave PA experiments have provided strong evidence for long-lived trapped charges in similar samples under visible photoexcitation [24].

Electric field effects in 1D excitonic systems have been predicted to include strong field-strength-dependent broadenings and spectral shifts [25]. Within the quadratic Stark effect description, the shift (ΔE_x) of the ground-state exciton energy (E_x) can be expressed as $\Delta E_x = \sum_j |\vec{\mu}_j \cdot \vec{F}|^2/(E_x - E_j)$, where $\vec{F}$ is the electric field strength and $\vec{\mu}_j$ and E_j are the dipole moment and energy of the continuum state j. The denominator of ΔE_x determines the sign of the shift, where coupling to higher- or lower-energy continuum states results in a red or blueshift, respectively. Here, autoionization of M-point excitons initially leads to a finite population of high-energy continuum

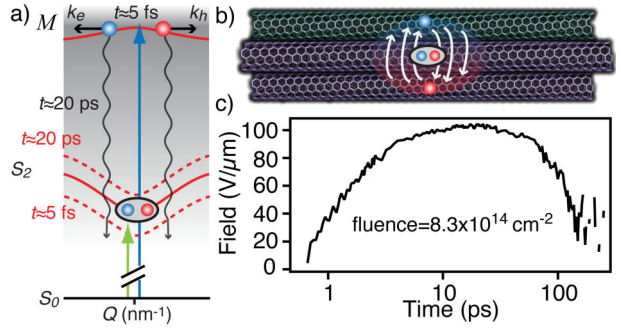

FIG. 4 (color). (a) Schematic of the electronic structure of a semiconducting SWNT with S_2 and the M-point exciton. The unperturbed S_2 exciton energy is given by the solid band. Early, ≈ 5 fs, dynamics upon UV photoexctitation lead to a red Stark shift of the S_2 exciton. Later dynamics, ≈ 20 ps, are where higher lying electron-hole pairs fully relax to energies below the S_2 exciton leading to a blue Stark shift. (b) Schematic of an internal field in a SWNT aggregate because of free charges in close proximity to an exciton. (c) Estimated field strength from the dynamic blueshift of S_2 described in the text.

states that redshift S_2. The buildup of a strong PA within 500 fs coincides with a sign change in ΔE_x; therefore, lower-energy continuum states within the energetic range of S_2 are populated after interband relaxation; see Fig. 4(a). Thus, we assign the PA to a broadening or enhanced dephasing of S_2 induced by hot free carriers. The slow recovery of ΔE_x to the S_2 ground-state energy reflects electron-hole pair recombination which occurs on a time scale of 100 s of ps. Moreover, the strong fluence dependence of the shift of the maximum PB in Fig. 3(d) is understood from the strong field dependence of ΔE_x, in which F is proportional to the local charge density excited by the pump pulse and stabilized within an aggregate; see Fig. 4(b). The magnitude of F can be estimated from the Stark shift of one-dimensional Wannier excitons, $\Delta E_x \approx 9e^2 r_0^2 F^2/8E_b$ [26], where $E_b = 350$ meV is the exciton binding energy and $r_0 = 1.0$ nm is the exciton radius; see Fig. 4(c). From the maximum blueshift of S_2 in Fig. 3(d), we estimated field strengths of up to $F \approx 100\ \mathrm{V}/\mu\mathrm{m}$, which is consistent with previous measured SWNT Stark shifts by the displacement photocurrent technique [27].

Concluding, we emphasize the importance of free-carrier transitions beyond an excitonic picture in describing the optical response of SWNT aggregates. Strong absorption strengths in the UV combined with exciton dissociation highlight an opportunity to further investigate related photovoltaic effects. Additionally, unusually large Franz-Keldysh oscillations at UV wavelengths in SWNTs have been previously observed by Ham *et al.* [28], and our findings provide a mechanism for generating the unbound electron-hole pairs that underline this behavior. In light of our findings, we expect that density gradient ultracentrifugation will be used as a tool to sort well-defined SWNT samples as a function of aggregate size to uncover systematic variations in excitonic and free-carrier responses [3]. Finally, we make the connection between a microscopic scattering mechanism and changes in the macroscopic dielectric function which alter the dimensionality of nearly ideal 1D semiconductors through an enhanced response of the underlying charge transfer continuum.

L. L. acknowledges support by the Spanish Ministry of Science and Innovation (Ramon y Cajal). This work was financially supported by the European Commission through the Human Potential Programme (Marie-Curie RTN BIMORE, Grant No. MRTN-CT-2006-035859) and performed, in part, at the Center for Integrated Nanotechnologies, a U.S. Department of Energy, Office of Basic Energy Sciences user facility.

*Present address: Physical Chemistry and Applied Spectroscopy, Los Alamos National Laboratory, NM 87545, USA.
jcrochet@lanl.gov
†Present address: Department of Material Science, University of Milano-Bicocca, Milan 20133, Italy.

[1] S. Reich, C. Thomsen, and J. Maultzsch, *Carbon Nanotubes: Basic Concepts and Physical Properties* (Wiley-VCH, Weinheim, 2004).
[2] K. Sato, R. Saito, J. Jiang, G. Dresselhaus, and M. S. Dresselhaus, Phys. Rev. B **76**, 195446 (2007).
[3] J. J. Crochet, J. D. Sau, J. G. Duque, S. K. Doorn, and M. L. Cohen, ACS Nano **5**, 2611 (2011).
[4] T. Ogawa and T. Takagahara, Phys. Rev. B **44**, 8138 (1991).
[5] Y. Takagi and S. Okada, Phys. Rev. B **79**, 233406 (2009).
[6] L. Yang, J. Deslippe, C.-H. Park, M. L. Cohen, and S. G. Louie, Phys. Rev. Lett. **103**, 186802 (2009).
[7] K. F. Mak, J. Shan, and T. F. Heinz, Phys. Rev. Lett. **106**, 046401 (2011).
[8] D.-H. Chae, T. Utikal, S. Weisenburger, H. Giessen, K. v. Klitzing, M. Lippitz, and J. Smet, Nano Lett. **11**, 1379 (2011).
[9] Y. Murakami and S. Maruyama, Phys. Rev. B **79**, 155445 (2009).
[10] M. C. Beard, J. L. Blackburn, and M. J. Heben, Nano Lett. **8**, 4238 (2008).
[11] J. Crochet, M. Clemens, and T. Hertel, J. Am. Chem. Soc. **129**, 8058 (2007).
[12] J. Crochet, M. Clemens, and T. Hertel, Phys. Status Solidi B **244**, 3964 (2007).
[13] K. De Blauwe, D. J. Mowbray, Y. Miyata, P. Ayala, H. Shiozawa, A. Rubio, P. Hoffmann, H. Kataura, and T. Pichler, Phys. Rev. B **82**, 125444 (2010).
[14] G. D. Scholes, ACS Nano **2**, 523 (2008).
[15] S. M. Bachilo, M. S. Strano, C. Kittrell, R. H. Hauge, R. E. Smalley, and R. B. Weisman, Science **298**, 2361 (2002).
[16] E. H. Haroz, S. M. Bachilo, R. B. Weisman, and S. K. Doorn, Phys. Rev. B **77**, 125405 (2008).

[17] L. Lüer, J. Crochet, T. Hertel, G. Cerullo, and G. Lanzani, ACS Nano **4**, 4265 (2010).
[18] C. Manzoni, A. Gambetta, E. Menna, M. Meneghetti, G. Lanzani, and G. Cerullo, Phys. Rev. Lett. **94**, 207401 (2005).
[19] S. Schmitt-Rink, D. S. Chemla, and D. A. B. Miller, Phys. Rev. B **32**, 6601 (1985).
[20] L. Schultheis, J. Kuhl, A. Honold, and C. W. Tu, Phys. Rev. Lett. **57**, 1635 (1986).
[21] L.-J. Li, R. J. Nicholas, R. S. Deacon, and P. A. Shields, Phys. Rev. Lett. **93**, 156104 (2004).
[22] D. Karaiskaj, C. Engtrakul, T. McDonald, M. J. Heben, and A. Mascarenhas, Phys. Rev. Lett. **96**, 106805 (2006).
[23] R. B. Capaz, C. D. Spataru, P. Tangney, M. L. Cohen, and S. G. Louie, Phys. Rev. Lett. **94**, 036801 (2005).
[24] C. Sciascia, J. Crochet, T. Hertel, and G. Lanzani, Eur. Phys. J. B **75**, 115 (2010).
[25] V. Perebeinos and P. Avouris, Nano Lett. **7**, 609 (2007).
[26] G. Weiser, Phys. Rev. B **45**, 14076 (1992).
[27] A. D. Mohite, P. Gopinath, H. M. Shah, and B. W. Alphenaar, Nano Lett. **8**, 142 (2008).
[28] M.-H. Ham, B.-S. Kong, W.-J. Kim, H.-T. Jung, and M. S. Strano, Phys. Rev. Lett. **102**, 047402 (2009).